26

Fiber-Optics in Scanning Optical Microscopy

Peter Delaney and Martin Harris

INTRODUCTION

Fifteen years ago, exploitation of fiber-optics in scanning confocal optical microscopy was minimal. Most practical applications relied upon technology derived quite directly from telecommunications applications (particularly the types of fibers themselves and the methods by which they were produced, packaged, and interfaced).

Since that time, there has been increasing acceptance of fiber components as illumination and detection elements in commercial scanning microscopes, and a marked increase in development of basic fiber technologies for scanning microscopy applications. Substantial progress has also been made in developing entirely new classes of highly miniaturized scanning confocal microscopes made possible only by fiber technologies.

Invention and production of more specialized optical fibers and fiber-optic devices has not only increased the practical opportunity to replace many of the conventional optical components with their more flexible fiber-optic counterparts, but in many cases has yielded completely novel and unique fiber components. Beyond the use of fiber-optic elements as efficient, flexible light conduits, fibers are now available that can act as spectral, spatial, and polarization filters, beam-splitters, lasers, and nonlinear devices for delivering light from pulsed lasers.

This chapter will introduce some of the relevant theoretical and practical parameters of fiber-optics, discuss these in the context of the role of fibers performing key functions within scanning microscopes, then move to a system-focused level that reviews the types of instruments that use fiber components and their capabilities and performance.

KEY FIBER TECHNOLOGIES RELEVANT TO SCANNING MICROSCOPY

Optical fibers with properties relevant to confocal microscopy range in complexity from slight variants of standard, telecommunications fiber through to novel fibers exploiting complex microstructures. An understanding of fiber design and function is pivotal to understanding their exploitation in scanning microscopes. We now overview the particular aspects of various fiber technologies that define their roles in various implementations of confocal microscopy.

Glass Made from Gas and Its Transmission Properties

Fiber technology is largely founded on production of ultra-pure glasses. This is achieved by creating glass from gas by bubbling hydrogen, oxygen, and helium through containers of volatile silicon tetrachloride, germanium tetrachloride, and, often, phosphorus and boron halide compounds. The vapor is burned to form a chalky, white deposit and further heating collapses this to produce an ultra-clear glass rod known as a preform. During this process, the composition of the vapor is varied to produce a specific cross-sectional refractive index profile. The preform is then melted and drawn down into fiber, jacketed for protection, and wound onto drums. Importantly, the drawing process preserves the cross-sectional profile of composition and associated refractive index (RI), and these are captured into the glass preform during its fabrication. Thus, simple or complex RI profiles can be made in the macroscopic domain (over many millimeters) of the preform, and subsequently become microscopic during the drawing process.

For the glass compositions most commonly used in optical fibers, the purity ensures that there is virtually no absorption of light during transmission for almost the entire wavelength range from 350 nm to 1600 nm (the transmission curve for silica glass is shown in Fig. 26.1). The predominant loss mechanism through this wavelength range is Raleigh scattering.

This transmission efficiency can be difficult to appreciate when working with the relatively short lengths of fiber used for microscopy applications. Although at wavelengths commonly used in scanning microscopy, losses in silica glass are orders of magnitude higher than at the wavelengths for which telecommunications fiber is commonly designed, telecommunications requires transmission over the 50 to 80 km distances between repeater stations. Thus, even for blue light over distances of several meters, losses are a fraction of a percentage. Inefficiencies in the optics used to launch the input (so-called insertion losses) or project the fiber output (e.g., excluding part of the Gaussian beam profile) are much more significant. If improperly managed, these losses can lead to the perception that fiber propagation is lossy.

Step Index and Gradient Index Optical Fibers

Some of the simplest optical fiber designs are comprised of a core of glass surrounded by a cladding of a different glass having a

Peter Delaney and Martin Harris • Optiscan Pty Ltd, Victoria 3149, Australia

Handbook of Biological Confocal Microscopy, Third Edition, edited by James B. Pawley, Springer Science+Business Media, LLC, New York, 2006.

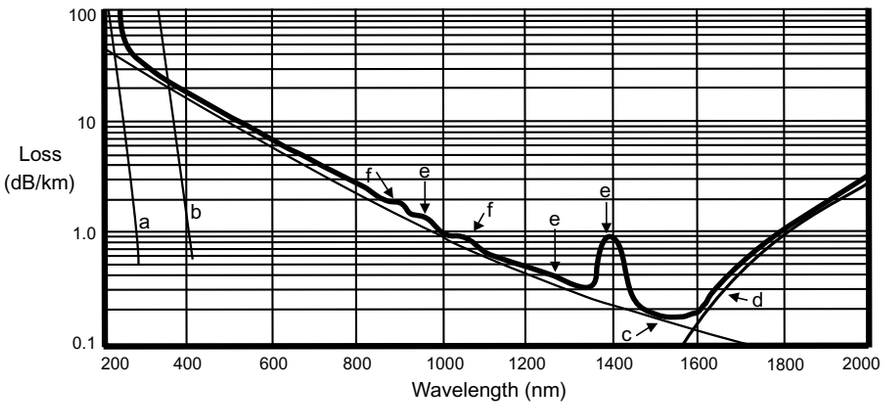

FIGURE 26.1. Transmission losses in silica glass optical fiber versus wavelength: (A) material bandgap absorption of silica; (B) material bandgap absorption of germania; (C) Raleigh scattering contributes loss mechanisms, which form bounding asymptotes to the overall shape of this spectrum; (D) infrared (IR) photon interactions; (E) absorption by residual water (OH bonds) in the glass superimpose several peaks in the spectrum; and (F) transition metal absorption bands.

lower refractive index (a so-called step index optical fiber). This forms a closed, cylindrical refractive index boundary that serves to entrap and propagate light by total internal reflection.

One of the properties of step index optical fibers is that the light that converges onto the input surface at higher angles must traverse a greater effective path length before it reaches the exit surface than light incident at lower angles. Hence, any pulse of light will be temporally dispersed. To overcome this limitation, gradient index optical fibers were developed (Wilson and Hawkes, 1989a). Gradient index fibers, as their name suggests, possess a gradient of RI from highest (at the center of the core) to that of the cladding [as depicted in Fig. 26.3(B)]. Rather than being reflected at an abrupt core/cladding boundary, the wavefront of light is steered continuously as it traverses the RI gradient. Light travels faster through the outer, lower RI medium, and hence tends to keep up with light propagating in the inner regions of the core, resulting in less temporal dispersion of the wavefronts of light propagated.

Modes in Optical Fibers

A propagating wavefront can interfere constructively or destructively with totally internally reflected regions of the same wavefront traveling across the fiber at a slightly different angle. Where this interference is constructive, the light propagates efficiently along the fiber. Hence, propagation of wavefronts at a particular wavelength is only supported for specific paths or angles within the fiber. These are called modes.

The modes that a given fiber will support are a function of the diameter of the fiber core d, the wavelength of light λ, and the RIs of the core and cladding, as well as the RI profile itself (in the case of gradient index fiber). An important parameter incorporating all these factors is called the V-number. The larger the V-number, the more modes a fiber will support, down to a cutoff value of V = 2.405, at which only a single, fundamental mode can be propagated by the fiber (Wilson and Hawkes, 1989b). This mode can be launched by focusing a train of converging concentric wavefronts to an appropriate diffraction-limited spot on the end of the core, and the light will then essentially propagate as a train of parallel wavefronts, as depicted in Figure 26.2. The light emergent at the output of such a fiber will also form a coherent virtual point source, radiating a train of diverging, concentric wavefronts analogous to laser light diverging from the waist region to which it has been focused, but with the numerical aperture (NA) of the fiber determining the angle of divergence. As will be discussed later, this ability of single-mode fibers to maintain coherence has many important properties relevant to their use in confocal microscopy. Importantly, when the V-number falls below the single-mode cutoff, the fiber still guides the fundamental mode. Note that V-number is related to wavelength in such a way that a fiber is single mode for all wavelengths longer than the wavelength associated with the single-mode cutoff. Thus, a fiber can be single mode across a range of wavelengths.

Modes can be visualized by viewing the far field projection of light emerging from a fiber (i.e., the appearance of the light output falling onto a piece of paper). For example, a large-cored step index fiber [such as depicted in Fig. 26.2] will be heavily multimode and may support hundreds or thousands of modes, which will appear as very fine spots that move rapidly with any disturbance to the fiber. Smaller-cored gradient-index fiber may support just a few modes and these will appear as characteristic lobes. The output of single-mode fiber appears as essentially a radially symmetric Gaussian-distributed disk.

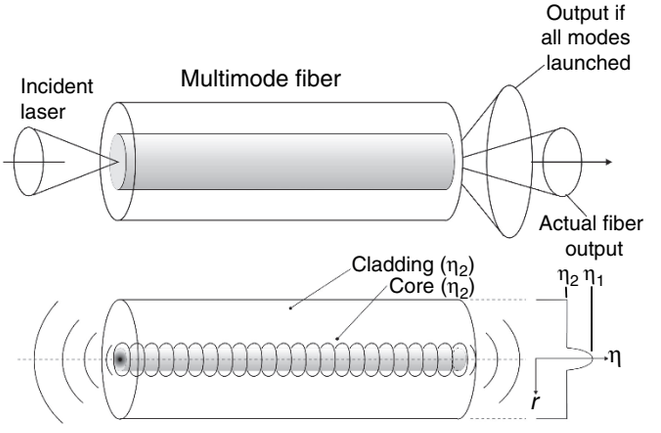

FIGURE 26.2. Diagrammatic representation of key differences between light propagation in step index multi-mode fiber and gradient index single-moded fiber. In a large core step index multi-moded fiber, the superset of all mode fields are confined to a cone which defines the NA of the fiber. The various modes allow propagation of light involving low through high angles of total internal reflection. It is possible to couple laser light into subsets of these modes. In the example depicted here, launching of laser light at lower than the maximum NA launches lower order modes, resulting in fiber output that is likewise lower in NA than that defined by the full set of modes supported by the fiber.

Evanescent Wave and Polarization Effects in Optical Fibers

When light is guided by total internal reflection from an RI gradient, a portion of the electromagnetic wave, called the evanescent wave, travels on the "far side" of the boundary (i.e., in the cladding) relative to where the mode is traveling. Correspondingly, an appreciable amount of the optical energy carried by a fiber is transmitted by the evanescent wave in the cladding surrounding the core, even for a step-index core.

The phase shift and lateral displacement that takes place when light is guided by the refractive index gradient is different for the two orthogonal polarization planes of the light. The distance that the evanescent wave penetrates into the cladding depends on the angle of incidence and the polarization state.

Light from lasers is usually linearly polarized. Conventional optical fiber has radial symmetry and if this symmetry were perfect and the fiber was held straight, then the polarization plane would not be changed during transmission. In practice, neither of these two conditions holds, so that the polarization plane of the emerging light may be rotated or it may be converted into a left- or right-handed circular or elliptically polarized beam. This is essentially uncontrolled in circular cross-section fiber.

Polarization-Maintaining Fibers

There are several designs of optical fiber that allow polarization to be maintained. It is either possible to make a fiber with an elliptical core cross-section or one with a circular core that is stressed by structures within the fiber but outside of the light-carrying core. These are made of a different glass type, which contracts more and produces stress in the core as the molten fiber cools. This stress produces a birefringence causing the speed of light traveling in the fiber in one polarization plane to differ from the speed in the other direction (by about 1 wavelength every millimeter of travel). This distance, called the beat length, is equivalent to a retardation in crystals and wave plates of one full wavelength. The phase between the two orthogonal polarization propagation modes thus changes back and forth and the coupling of energy from one polarization mode that occurs in one half beat length is reversed in the next half beat (hence little net change results). These so-called high birefringence (Hi-Bi) fibers can be bent without altering the polarization state of the output light. Two common designs of stressed fiber are called, descriptively, Panda and Bow Tie fibers (see diagrams in Fig. 26.3). The Panda fiber is made by drilling holes in the preform on either side of the core and inserting rods of glass having a higher thermal expansion coefficient before the fiber is drawn. The Bow Tie and elliptical core structures are made as the preform is deposited from the gas. When using polarization-maintaining fibers in some applications, it is critically important to ensure that the laser launch polarization is aligned with either the fast or the slow axis of the fiber. Rotating the fiber exit tip will rotate the polarization plane by exactly the same angle and this can be employed to align polarization when setting up experiments. It also should be pointed out that each of the modes in a multimode fiber can have its own separate linear polarization state. Failure to perform alignment correctly can cause large variations (commonly from 30% to 80%, but up to 100%) in the delivery of the desired polarization mode into the microscope. In some cases, this can be monitored by direct power measurements at the objective, or, more generally, by evaluating the images of a stable test specimen such as a mirror. Note that swings in polarization mode might not be measurable directly at the fiber output, as the light may still be coupled into a non-desired polarization mode, and the polarization change may only become evident as an intensity change after the light interacts with microscope or detection components that are polarization dependent. Any significant swings in these observations (more than a few percentage points) should flag the possible need to realign the fiber launch and/or alignment of the fiber output to the microscope.

Fused Biconical Taper Couplers: Fiber-Optic Beam-Splitters

If two sections of optical fiber are fused together and then stretched while still viscous, the cores are tapered, thinned out, and brought very close together. Each core overlaps significantly with the evanescent wave associated with light guided by the other. This allows light energy to be transferred from one core to the other, forming a type of beam-splitter. Such devices are called fused biconical taper couplers (FBTCs) [Fig. 26.4(A)], and may fit into a capsule the size of a match. They have been manufactured with net optical power losses of less than 0.01%. The theory covering the division of the light is not intuitive and is covered in Snyder and Love (1983). These couplers can produce a 50 : 50 division of the the light or any other desired ratio.

Although the split ratio of any FBTC varies with λ, couplers can be fabricated to be relatively λ-independent or highly λ-dependent. In the latter case, they can be used as dichroic beam-splitters [Figure 26.4(B)]. They can also be made to split the incoming light from one fiber so that light with orthogonal polarization modes emerges from the two output legs of the coupler. Alternatively, they can split light in a ratio that is independent of the polarization plane (Wilson and Hawkes, 1989c).

FBTCs can be used to combine the light from separate laser sources and they can also function as beam-splitters in confocal microscopy, where they offer additional modularity by providing separate fiber arms for laser launch, fiber output, and signal detection. They have also been a key component in making optical

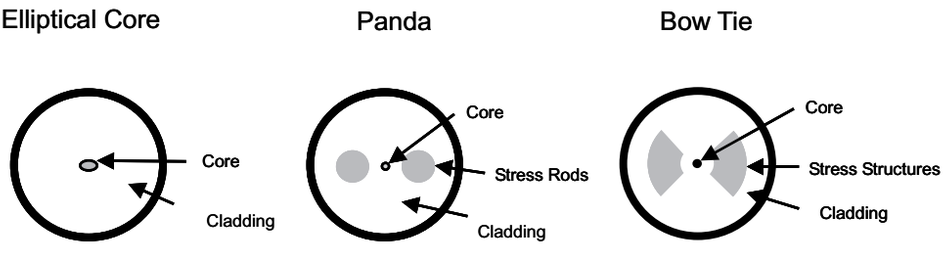

FIGURE 26.3. Polarization maintaining fiber core patterns. Various means are pictured whereby specific core profiles and stress structures are fabricated into a fiber preform prior to drawing. This results in an orthogonally biased pair of modes, each favoring one linear polarization plane.

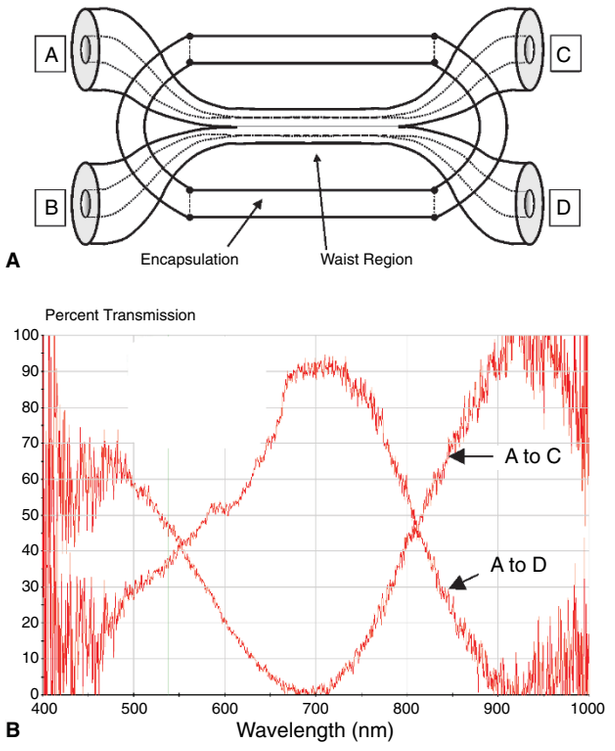

FIGURE 26.4. Fused biconical taper couplers. The general configuration is shown in (A), whereby two fibers are melted together and drawn, forming a waist region in which the mode fields guided by the cores overlap and exchange energy. Laser light coupled into any arm of the coupler will be apportioned in the two opposing arms in a ratio that is dependent upon the wavelength characteristics of the coupler, which can be varied by design. An example is given in (B) for a coupler with strong wavelength dependence that could be used, for example, to provide a 50 : 50 split for laser illumination at 488 nm, while favoring the transmission of confocal green fluorescence emission on one particular arm. Thus, the coupler could be used as for laser illumination, pinhole detection, and a dichroic beam-splitter in a fiber-based confocal microscope.

coherence tomography a useful *in vivo* imaging technique, where they provide the beam-splitting and recombination paths for the requisite interferometer (OCT; see also Chapter 34, *this volume*). One of the advantages in these applications is that fiber-based interferometers are not troubled by dust, as are conventional interferometers.

Microstructure Fibers

New designs of fibers, collectively called microstructure-core fibers (but also referred to as photonic crystals, air-clad fibers, or endlessly single-mode fibers, etc.) have recently been introduced. The cross-sectional views of several such designs are presented in Figure 26.5. Rather than exploiting a simple radially symmetric refractive index profile to guide light, these fibers consist of complex patterns of air holes and glass fins.

These structures give rise to unique optical properties, in particular nonlinear propagation effects that are not handled well by the conventional descriptors of linear modes in cylindrical fibers. Some of these fibers [see Fig. 26.5(A,E)] suspend what is effectively a large fiber core in a web of glass supports. Others [Fig. 26.5(B–F)] have a series of thin tubes around a hollow core. Although this pattern appears to defy the theory of conducting light by total internal reflection (TIR) in a high-RI core, they can be understood as Bragg-grating mirrors/photonic bandgap structures, surrounding and guiding the wave energy. The light is trapped between mirror structures in the cladding formed by the surfaces of the regular array of holes. Common examples of intrinsically colorless, transparent, multi-layer structures that act as mirrors include the reflective skin cells of fish, gel holograms, and the iridescent scales on butterfly wings. Applications of these fibers will be discussed in the context of optical fiber illumination.

Fiber Image Transfer Bundles

Coherent image transfer bundles are one of the earliest applications of optical fibers. Tens or hundreds of thousands of fibers are

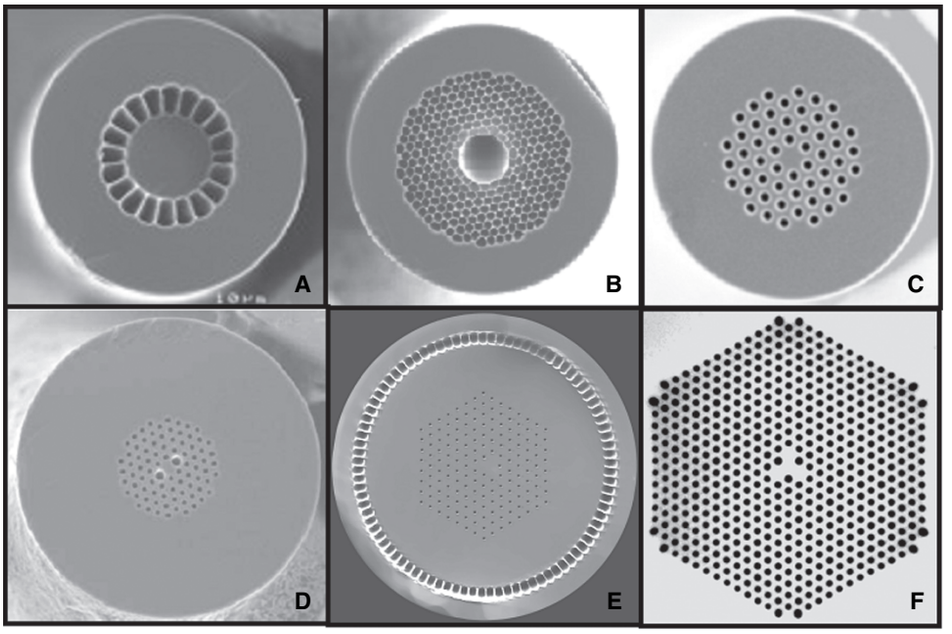

FIGURE 26.5. Images of the profiles of various microstructured optical fiber. Air cored fibers (B–E) exhibit low or negligible chromatic dispersion, whereas air cladding structures (A), and in a hybrid with an air core (E and F) can be pre-reverse chirped to excite nonlinear modes of propagation of ultra-short, high peak power pulses. The two larger air cores in (D) give this fiber polarization-preserving properties.

combined in a bundle, each fiber transferring one spot of light from a focused image at one end of the bundle to an identical configuration of fiber tips at the opposite end. This process reconstitutes the image. Invented by Logie-Baird in 1927, fiber-optical bundles were widely used for internal endoscopy after the 1950s, but now have largely been replaced by miniature solid-state video cameras. These devices present particular issues in terms of the way that they sample the image plane to be transferred. Because the fiber cores are separated by the cladding regions (unavoidable if the cores are to guide light), the image plane is sampled only at discrete locations. This complicates the interpretation of their performance and will be discussed below in more detail in the context of the microscope configurations that exploit them.

Two processes are commonly used to make coherent image transfer bundles. Fibers or preform rods with high RI centers can be packed together in a hexagonal pattern and then fused and drawn out. The hexagonal array and RI pattern are maintained in miniature form during the drawing. This process may be repeated if a smaller core is required. Alternatively, coherent bundles can be formed by winding very thin fibers on a mandrel, gluing together all the fibers in one section, and then cutting through and polishing both ends of that section. Bundles of fiber made by the latter method are as flexible as a hank of silk. Fused bundles are generally stiffer.

KEY FUNCTIONS OF FIBERS IN OPTICAL MICROSCOPES

Fiber technologies are presently exploited in various instruments including confocal microscopes, OCT scanners, and laser scanning nonlinear microscopy systems. Most of these applications involve the use of fibers, either for remote laser delivery and/or as a detection aperture and some use fibers that serve both these functions simultaneously. The major factors important in such systems are (1) the efficient launch of laser light into the optical fiber; (2) proper handling of the fiber output as a light source; (3) efficient projection of the returning signal light onto a fiber that is acting as a detector aperture; and (4) transmission of short pulses suitable for nonlinear microscopy. Note that these functions are not necessarily independent.

Optical Fiber for Delivering Light

The use of optical fibers as flexible laser delivery systems has been established for many years, proving particularly useful in medical laser delivery [e.g., in "laser knife" surgery or laser ablation of skin blemishes (Katzir, 1993)]. Among the major advantages to be gained by fiber-optic light delivery are the isolation of bulky laser equipment (including vibration isolation) and the flexibility provided by being able to actually handle and manipulate the laser output (e.g., in hand-held laser cutting devices). The properties of the output depends both on key fiber parameters (e.g., RI gradient, V-number) and those of the coupled laser (modes, wavelength, etc.).

The most common application of optical fibers in confocal microscopy is the use of a single-mode laser beam coupled to an optical fiber that is single-mode at the laser wavelength(s).

Factors important to efficient coupling of laser light into an optical fiber include: the beam profile and polarization of the laser, the mode profile of the fiber, its NA and, in the case of a pol-preserving fiber, its orientation, and the relative position of the lens system used to project the laser output into the fiber core. The key requirement is to focus the beam onto the fiber in a manner that achieves maximum overlap between the distribution of energy in the focused spot and the modal field that exists near the fiber tip, that is, there must be a complete overlap between the focused beam and the acceptance cone of the fiber. In practical terms, this means that the beam to be launched into the fiber must itself be everywhere coincident with the light that would emerge from the fiber had it been launched from the opposite end. Indeed, actually back launching a small amount of light in this manner serves as a very useful tool in the alignment of a laser/fiber coupling apparatus.

Many devices for launching laser light into optical fibers consist of a lens holder that can be aligned to the laser beam and a means of positioning an optical fiber at the focused spot, including an adjustment of its tilt. Orienting the fiber to maximize light throughput will in general correspond with translational alignment of the spot onto the fiber core (Figure 26.6). However, Figure 26.6 also shows that this will not necessarily be sufficient to ensure maximum coupling efficiency as this also requires both perfect axial (tilt) alignment and matching of the NA of the fiber with that of the incident, converging wavefront (Fig. 26.6).

Although the Gaussian beam profile of single-mode transverse electromagnetic mode (TEM_{00}) lasers is typically well matched (but not perfectly) to the modal field of single-mode optical fiber (Snyder and Love, 1983), the output from a solid-state laser is typically asymmetric and astigmatic unless corrected with dedicated anamorphic lenses. If the lens system is very well corrected for the application and meticulously aligned, coupling efficiency of approximately 90% is possible; however, with commonly available components (dedicated lens systems that are commercially available for common laser and fiber types) 60% to 70% should be routinely expected.

Instabilities in the output power can be caused by instability in any of the parameters mentioned above as being important to efficient launch.

Consideration should also be given to the light that is not propagated in the core of the fiber. For an air-to-fiber launch, approximately 4% will be lost at the air–glass interface by Fresnel reflection (assuming the fiber end has no anti-reflection coatings). Light that enters the fiber but is not propagated in modes will travel short distances in the cladding (centimeters to tens of centimeters)

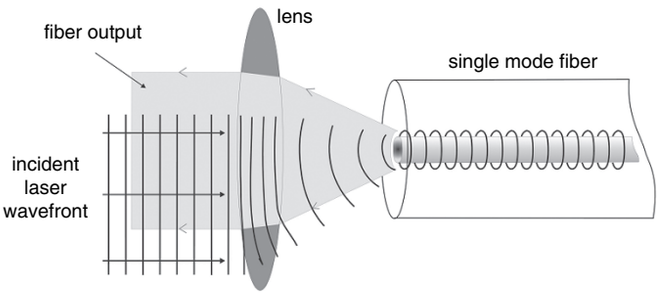

FIGURE 26.6. Single-mode fiber launch. Efficient coupling of a TEM_{00} laser beam into a single-mode fiber requires optimization of multiple degrees of freedom. First, the beam must be focused onto the core region. Second, the beam NA must be matched to the fiber NA and the axis of the convergent cone of light must be aligned with the mode field of the fiber. The incident beam in the diagram that is not overlapping with the mode field of the fiber will not be coupled into the fundamental mode, and will be radiated away over a short distance of fiber.

before being entirely radiated away, and will generally have a negligible impact on the output of fibers having lengths typical of those used for microscope illumination. However, the unguided light can excite fluorescence in fiber jacketing materials, a very small proportion of which may be propagated and contribute to background in the optical path of the microscope. Careful selection of non-fluorescent materials for fiber jacketing (particularly near the launch end) can eliminate this problem.

As discussed previously, the emergent light will be a series of concentric, diverging wavefronts, as though from a focused point of laser light. These spherical waves can then be re-collimated to provide a beam having the characteristics of a pure, fundamental-mode laser beam. Note that although collimation may only be required for certain applications, the preservation of this coherent laser wavefront is a critical optical property that affects all subsequent handling and propagation of the beam. When the output is projected into an optical system such as a confocal microscope, the output of the single-mode optical fiber is best considered to be equivalent to a TEM_{00} laser beam diverging from the point at which it is focused.

In contrast, if a multimode fiber is used for laser delivery, the different modes will act as a series of light sources or pinholes, each of which will image to a separate spot within the specimen. Note, however, that in a practical situation, the number of possible modes that actually propagate light is very sensitive to the launch conditions (it is often possible to launch only the fundamental mode or a limited subset of modes in a multimode fiber by careful launch alignment). Coupling efficiency for launching laser light into the fundamental mode of a few-mode fiber is comparable to that for single-mode fiber. The treatment of single-mode optical fiber output as a coherent point source cannot be accurately generalized to the case of a multimode fiber. Although each of the different individual modes will still maintain coherence, the overall output will be the sum of all modes propagated. The most important difference will generally be that the output can neither be restored to a single, parallel wavefront, nor focused to a diffraction-limited spot.

Optical Fiber as a Detection Aperture

The use of optical fiber as a detection aperture offers the potential for transmitting the signal light returning from the specimen to an external detector. The detectors themselves may include specialized devices such as spectrometers as well as the more common photomultiplier tube. The intrinsic properties of the single-mode fiber allow it to provide imaging characteristics similar to those of a conventional pinhole detector. The core size is related to the NA of the beam entering it in the same manner but it is defined in terms of the soft edges of a Gaussian mode field, instead of the abrupt edges of a physical pinhole in an opaque material (i.e., the edges of the "virtual" pinhole are fuzzy).

Single-mode, few-mode, and multi-mode fibers can also act as coherent detectors. This has been demonstrated for the case of a two-mode optical fiber, for which differential measurement of the modes permits phase-contrast imaging of surfaces with very accurate height determination (Kimura and Wilson, 1991; Wilson *et al*., 1992).

The spatial distribution of modes within a multimode detection fiber may also carry information regarding the source of the signal. For example, spatial filtering of light from the near field or the far field projection of the fiber can mimic the role of a variable detection aperture. A rather elegant example uses the difference in RI coefficients between silica glass and the silicone elastomer jacket to form a temperature-tuned variable pinhole with no moving parts. (Harris and Delaney, patent). The variation in pinhole function achievable by this approach is dependent upon the number of modes supported by the fiber, and the extent to which the coupling optics distribute light into these modes. It is possible to control the effective pinhole size continuously from that of a single-mode fiber up to a large-core multimode fiber, or a change of several times in effective pinhole diameter. This approach is applicable to single fibers only and not to fiber bundles.

Same Fiber for Both Source and Confocal Detection

The use of a single fiber as both the source and detection aperture best exploits the potential for fibers to offer stability and robustness in alignment, as well as to enable miniaturization of the imaging head. This made it possible to construct compact scanning heads to mount on microscopes as well as highly miniaturized imaging heads (both in single-fiber and fiber bundle configurations, see below).

One technical difficulty in implementing any approach whereby light is detected from the illuminating fiber (as in a single-optical-fiber confocal microscope; Delaney *et al*., 1994a) relates to the fact that both ends of the fiber are in image planes of the microscope. As a result reflections of the excitation light that are generated at the fiber tip must be suppressed. Fresnel reflection of the incident laser at optical surfaces can direct a significant amount of light into the detection path. As a result, careful management of launch conditions becomes critical for reasons other than efficiency, as it represents a source of background noise or artifacts. Both the launch efficiency itself and the control of light scattering at both fiber ends assume paramount importance.

Standard methods commonly used to manage insertion losses in telecommunications fibers can be applied directly to these situations:

- Angle polishing of fiber tips so that the reflected portion of the launched laser is reflected along a separate path than the mode field of the fiber (i.e., the path that light emerging from the fiber will follow). Any light to be measured back through this fiber can thus be spatially separated from the reflected light. Angle polishing can also be used to suppress return loss from the distal endface because the light reflecting back from the angled surface will not be aligned with that in the propagated mode.
- Index matching of fiber or bundle terminations (e.g., by filling the space between the launch optics and the fiber tip with an immersion medium). This minimizes or eliminates reflections that occur at an air–glass refractive index boundary, or deflects them away from the detection path.
- Anti-reflection coating the fiber tips.

Other sources of background include Raman generation in the fiber core and fluorescence from the polymers used in the fiber coating and connectors. Careful selection of fiber jacketing and the materials used in connectors (including glues) is essential if one is to minimize sources of stray light. If handled carefully, background levels 5 to 6 orders of magnitude below the incident laser power are achievable.

Note that, as polarization sensitivity of modes may confound efficient detection of the randomly polarized fluorescence signal (e.g., from unbound fluorescent probes), systems based on this design tend to use optical fibers that are not polarization-preserving.

Fiber Delivery for Nonlinear Microscopy with Femtosecond Lasers

Two-photon, three-photon, and allied nonlinear microscopy requires ultra-short (femtosecond domain) pulses delivered at very high peak optical powers to generate second- and third-order effects. Although titanium–sapphire femtosecond lasers are widely employed for this purpose with direct beam delivery, the use of fibers to transmit the pulses would provide greater convenience if a number of difficult technical challenges can be overcome. Short pulses necessarily contain a small range of wavelengths (10 nm at 100 fs, white light at 1 fs). Once the pulse is in the fiber, chromatic dispersion (due to different wavelengths propagating at different speeds) causes the shorter wavelength components to lag those with longer wavelength. This makes the pulse last longer. For example, a 50 fs pulse [which has a spectral spread of around 20 nm full-width half-maximum (FWHM)] can spread to several picoseconds in the process of traversing a meter of fiber. Some investigators have attempted to overcome this problem by using a device known as a pre-reverse chirper to progressively delay the longer wavelengths relative to the shorter wavelengths. Thus, the slower-traveling blue components gain a head start on the faster-traveling red components. If tuned correctly, the faster red components catch up to the slower blue just as they reach the end of the fiber, reconstituting the original short pulse at their target destination in the sample.

Although elegant, this approach has two limitations. First, it does not deal with a secondary spectrum, which is not so easily corrected. Second, even if the chromatic dispersion is perfectly corrected, the presence of high peak powers concentrated into a tiny fiber core can alter its function of, or even destroy it (Fork *et al*., 1984).

Although pre-reverse chirping can result in fiber delivery of pulses short enough to excite two-photon fluorescence, the limitations of pulse restoration and peak power have prevented such systems from imaging specimens to a greater depth than single-photon confocal microscopy, thus negating the benefit of nonlinear excitation. However, various microstructure fibers now hold much promise for bringing practical fiber-optic illumination to nonlinear optical microscopy.

Some classes of air-core optical fiber have been shown to have virtually zero chromatic dispersion and are also capable of transmitting high power levels (Knight *et al.*, 1998; Bjarklev *et al.*, 2003). Other fibers that suspend a large central core by a fine structure of spokes have been shown to be capable of transmitting 140 fs pulses at high peak power (Ouzounov *et al.*, 2002).

Some of these nonlinear effects are caused by the fact that the pulse intensity is so high that it locally changes the RI of the glass and allows the trailing part of the wave to catch up in a process called self-phase modulation. This can generate ultra-short isolated wave sets called optical solitons, which are able to travel in such fibers over considerable distances without spreading. The process is analogous to that which produces tidal bores in some estuaries.

Not surprisingly, microstructured fibers demonstrate different properties for the linear propagation of continuous light energy than for the nonlinear propagation of pulsed energy. In particular, some feature very large core diameters that are massively multimode in the linear domain. Thus, they may function as a large area detection pinhole. This may be appealing in many nonlinear microscopy applications because nonlinear illumination can be combined with non-confocal linear detection using the same fiber.

Large Core Fibers as Source or Detection Apertures

In addition to their function as a point source or a detection aperture, optical fibers can also provide diffuse illumination and large area detection.

For example, very large fluid-core fibers can scramble the spatial or temporal structure of arc or filament light sources with the result that the endface of the core serves as a uniform, diffuse source (Ellis, 1985) (as described in Chapter 6, *this volume*).

Likewise, large-core fibers can be used to carry the signal light passing through a physical pinhole aperture in the scan head to a remotely mounted photodetector. When used in this fashion, it is important to remember that, no matter how sophisticated the optics used to magnify or demagnify the semi-coherent light coming through the pinhole, one cannot demagnify the original source of the signal without losing photons. Therefore, the distal end of the fiber must always be at least as large as the source of light in the specimen and, were such a fiber to be used as a collector for non-descanned detection in nonlinear microscopy, its input surface should be larger than the area of the **raster** scanned in the specimen.

BENCHTOP SCANNING MICROSCOPES EXPLOITING FIBER COMPONENTS

Single-mode fiber-optic laser delivery is almost standard on modern commercial laser scanning confocal microscopes. Over several design generations, this has enabled the design of more compact scanning heads, eliminated laser vibration from the microscope stand, and increased the flexibility in laser delivery, although fused biconical taper couplers are not yet commonly used for mixing the outputs from multiple lasers.

Most systems require control of the polarization state of the laser illumination for multiple reasons. First, the quarter-wave-plate antiflex systems for suppressing specular reflections from lens surfaces are polarization dependent (see Chapter 7, *this volume*). Second, as the split ratio of the 45° reflecting surface in beam-splitter cubes exhibits strong polarization dependence, any change in beam polarization can produce significant changes in the excitation power delivered to the specimen. Third, differential interference contrast (DIC) and other contrast techniques require a fixed, linear polarization state. Consequently, most laser-scanning confocal microscopes deliver the laser light with polarization-maintaining fibers. Due to their specialized core profiles (Fig. 26.3), polarization-maintaining fibers can support each of two polarization-dependant modes and act as a single-mode fiber for each of them. Hence, when properly coupled to a linearly polarized laser source, they act as a single-mode fiber.

At different times, several systems have also been produced that utilize fiber-optics on the detection path, enabling modularization of the detection scheme.

The use of one fiber for illumination and another for detection offers a high degree of modularity and flexibility (e.g., as exploited in the Nikon C1 system). This has been employed in a system for confocal micro-Raman imaging (Sharonov *et al*., 1992), offering great flexibility in laser sources and detection components.

Incorporation of fiber delivery in multi-photon microscopes has remained a niche field for many of the reasons described above. Although there have been numerous attempts to modify commercial laser-scanning microscopes to accept fiber-delivered pulsed light sources using reverse pre-chirping and a standard

cylindrical fiber, these have remained limited to applications requiring longer pulse lengths and lower peak powers. Such systems have not provided the deep tissue imaging and flexibility in multi-photon excitation cross-section common from conventional systems.

Now, however, microstructure fiber is rapidly being applied to this area and early data suggests exciting progress. With these advances, fiber delivery will be increasingly adopted for nonlinear microscopy in experimental and commercial systems. This will allow novel configurations and the development of miniaturized scanning systems, such as those already available in confocal microscopy.

MINIATURIZED SCANNING CONFOCAL MICROSCOPE IMAGING HEADS

The most basic properties of confocal microscopy suggest numerous applications involving microscopic imaging of living tissue *in vivo*. In particular, the transition of biomedical research from bench to bedside faces numerous obstacles in understanding biological and morphological events in complex living systems on a microscopic scale. Until now, relatively few applications have been realized due in no small part to the cumbersome nature of bench-based microscope configurations. The development of miniaturized, scanning-probe devices suitable for practical *in vivo* confocal microscopy has long been a goal. The requirements of a miniature confocal imaging head for *in vivo* microscopy are small diameter (one to several millimeters), short rigid length (millimeters to several centimeters), and flexible umbilical connection to the rest of the instrument. In some applications (particularly in clinical medicine), there are further requirements for compatibility with conventional endoscope components and for disinfection or sterilization.

Fiber-optic technologies have played an enabling role in these developments, some of which have led to practical products and medical devices that employ various optical schema, as depicted in Figure 26.7 and described below.

Miniature Confocal Imaging Heads Based on Coherent Imaging Bundles

Coherent imaging fiber bundles present an intriguing range of trade-offs between the need for image quality versus simplicity of miniaturization and implementation.

A coherent fiber-optic imaging bundle can be used to transfer the scanned image plane from an open location to one with spatial constraints [i.e., one mounted on an endoscope; Gmitro and Aziz, 1993; Fig. 26.6(A)]. The focused laser beam is scanned across the proximal surface of the bundle injecting light sequentially into each of the fibers. Each fiber can then act as a confocal pinhole, returning light from the field on which its projection is focused in the sample.

Such a microscope can operate in a contact mode in which the polished end of the fiber bundle defines the image-isolation plane by directly touching the tissue. Alternatively, an appropriate lens can be mounted distal to the exit surface of the bundle to allow the projected image of the scanned spot or line to be refocused onto the specimen to obtain confocal images. In this case, any individual fiber in the bundle functions in a manner equivalent to the single fiber in Figure 42.6B as described in the next section. Contact imaging provides the smallest practicable endomicroscope but the resolution is effectively limited by the physical spacing of the fibers (~5 μm). The second method can have a higher resolution if the projected image of the fiber bundle is de-magnified by the lens system (Fig. 42.7, insert).

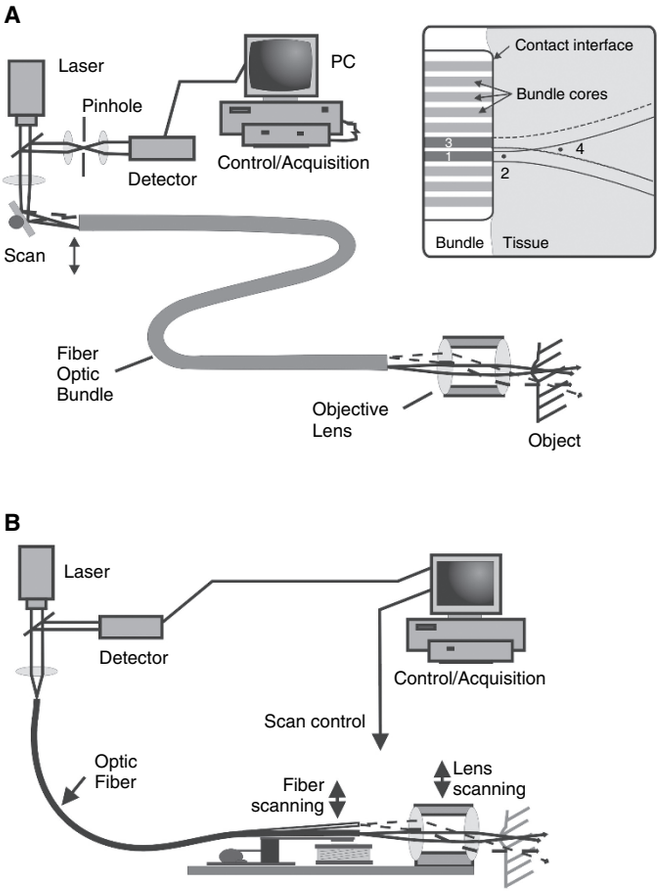

FIGURE 26.7. Optical schema for miniaturized confocal microscopy systems and heads. (A) Scanning the proximal end of a coherent fiber bundle transfers the illumination sequentially to the fibers in the bundle. The light emerging from one or more fibers is coupled to the tissue either by a lens system (main diagram) or by direct tissue contact (inset). In the former case (main diagram), the design of the lens system dictates the resolution achieved for imaging the specimen, and in particular how the discontinuous nature of the bundle impacts the optical sampling of the tissue (see main text). In the latter case, light emergent from a given core in the bundle (e.g., core 1, inset) will illuminate its mode field in the tissue. A near field point (2, inset) in the mode field will return light to core 1, but not to adjacent cores. Slightly further from the end of the bundle, points illuminated by core 1 (point 4, inset) can return light both to the illuminating core 1 and to adjacent core 4. Thus, the sampling of the tissue is governed by the NA of the fibers, scattering in the tissue, and the geometry of the bundle. (B) A single fiber is used as the illumination source and confocal detection path aperture, coupled to the focus in the tissue by a miniature lens system. Scanning can then be achieved by a variety of means. The fiber can be physically scanned relative to a laterally fixed lens, or the fiber can be fixed and the lens itself laterally scanned. Alternatively, the fiber and lens can be fixed and scanning performed by micromirror devices, or microlenses fitted to the tip of the fiber itself, which are scanned together (not shown).

Although sampling artifacts can occur when the hexagonal pattern of the fibers is imaged onto the CCD, to reveal the black cladding around each core, this can be overcome by software processing to reconstitute the signals from the individual fibers, producing an image that appears continuous [as it does, for instance, in the Mauna Kea Technologies system (Paris, France) (see Fig. 42.9].

However, such correction does not address the potential undersampling in the objective imaging-plane, where the output of each fiber (and its corresponding detected field) is discrete from that interrogated by neighboring fibers.

A successful optical-sampling system would not waste any light, and would both illuminate the focus plane in the object uniformly and project the image of an in-focus point object so that it is at least 4 core-spacings wide when it strikes the distal end of the fiber bundle (see Chapter 4 about sampling, *this volume*).

Several interacting operational variables affect this sampling problem and its impact on photon efficiency: packing the fibers more closely at the bundle output requires the use of high-RI glass cores and this results in the fiber having a higher NA and therefore emitting light into a larger spot at the BFP of the objective. If the NA of the fiber is larger than the back-NA of the objective [$NA_{back} = NA_{front}$]/M, where M is the (de)magnification], then much of the excitation light emerging from the fiber core will miss the objective. This reduces the photon efficiency in proportion to the square of the ratio of the respective NAs.

The objective lens system itself has both a magnification and an NA. As long as the BFP is filled, a larger NA implies smaller spots in the focus plane,[1] and consequently makes it more likely that the focused spots will not overlap. Higher demagnification not only implies a lower NA_{back}, but also ensures, that for a given fiber spacing, the spots at the focus plane in the specimen will be closer together.

The optimization depends heavily on the properties of the bundle. The most suitable bundles are densely packed, and consist of cores of approximately 4 µm diameter with a center-to-center fiber spacing of approximately 6 µm (i.e., the cladding between is ~2 µm). This yields a high-density 30,000 element bundle that is about 2 mm in diameter, including the jacket. If the cores get much smaller, they begin to act as single-mode fibers, especially at longer wavelengths, slightly reducing their throughput of incoherent fluorescent light. If the cladding gets much thinner, light begins to leak to adjacent fibers. To reduce this effect, the-core-to-cladding RI difference must be made as high as possible, resulting in a high fiber NA (0.3–0.4, versus NA 0.1–0.15 for communication fiber). As the NA of the objective varies between 0.4 and 0.5, operation at a magnification as low as 5× will still reduce the back NA to ~0.1, meaning that only 1/16 of the light emitted by a 0.4 NA fiber will strike it: 10× operation would be 4× worse.

A 0.5 NA objective demagnifying 488 nm light emerging from a bundle with 5 µm spacing by 10 : 1 will produce spots of that are ~0.75 µm at FWHM on a 0.5 µm spacing in the focus plane. These spots should overlap fairly well, and when the scanning system scans the laser beam over the proximal surface of the bundle, sequentially illuminating the cores on the distal surface, the entire focus plane will eventually be excited. However, any fluorescent or scattered light from an in-focus point object that returns through the objective, will form an image with a FWHM of only 5 µm in diameter at the fiber bundle surface. This is two times smaller than it should be to be sampled by at least 2 measurements (i.e., 2 cores across the FWHM, 4 cores across its entire diameter) as is required by Nyquist.

As with any form of undersampling, it can be overcome by increasing the sampling frequency (i.e., increasing the optical magnification or decreasing the core spacing) to meet the Nyquist criterion. Alternatively, one can "spoil the optical resolution," perhaps by introducing aberrations into the optics. As a result, energy from each fiber will be spread over a larger area in the specimen and the returning confocal signal will again be further defocused on its way back to the bundle. This results in some light striking adjacent fibers, achieving a similar result to increasing the sampling rate. It was employed by the authors in the prototype constructed to obtain Figures 42.8E and 42.8F.

Because any method used to overcome this problem necessarily involves mismatching the NAs of the fiber and the optical system, substantial reductions (i.e., from 90–99%) in photon efficiency cannot be avoided. The optimization and compromises depend heavily on the properties of the bundle.

Resolution and Optical Efficiency of Bundles

It can be seen from the above that the resolution achievable with a bundle system cannot be directly derived from the number and spacing of the fibers in the bundle and the objective lens magnification and NA. For a properly sampled objective space, several fibers are required per objective resel. A properly matched laser system can achieve a 70% launch efficiency into a single core, but measurements show that the light throughput drops to ~20% when the spot is defocused to cover several fibers at the polished end of a bundle. From geometrical arguments, it follows that if Nyquist-sampled resolution is required, then a considerable amount of excitation light (>75%) will be lost due to overfilling and around 70% of the confocal return is lost at the cladding interface.

As with any fiber-based confocal system involving illumination and detection via the same fiber, end-face reflections and fluorescence from the fibers or associated packaging may give rise to artifactual background signal. As with single-fiber confocal systems, these reflections may be minimized using the same techniques as those exploited in telecommunications (i.e., refractive index matching). Images from the Mauna Kea bundle system show effective removal of the fiber bundle autofluorescence pattern. This may be achieved by first using a high degree of over-sampling to properly capture the fine structure of the pattern, and then subtracting the fluorescence pattern from the bundle from the raw tissue data sets.

Bundle Imagers for *In Vivo* Studies in Animals

Despite the above compromises, the imaging probes that have been produced using bundles have produced the smallest confocal microscopes. Probes range from approximately 0.3 to several millimeters in diameter, and produce images with several thousand to several tens of thousands of resels per image. Bundle probes are thus well suited to *in vivo* microscopy in small animal models, and potentially in clinical applications that require access to very small orifices. For example, these devices enable colonoscopy in mouse models of early colorectal cancer formation, permitting longitudinal studies of individual tumors (Cavé *et al.*, 2005). A range of examples of animal tissues examined using miniature fiber-bundle confocal microscopes is presented in Figure 26.9.

[1] This illustrative calculation assumes that the light emerging from each core is fully coherent (i.e., that the fiber supports only a single mode). Because the fibers are actually multimode, the size of spots in the focus plane is not directly proportional to the NA and they are actually somewhat larger than stated. However, on the return journey, correct fiber spacing, not fiber size, is the parameter required to properly sample the magnified image of an in-focus point object.

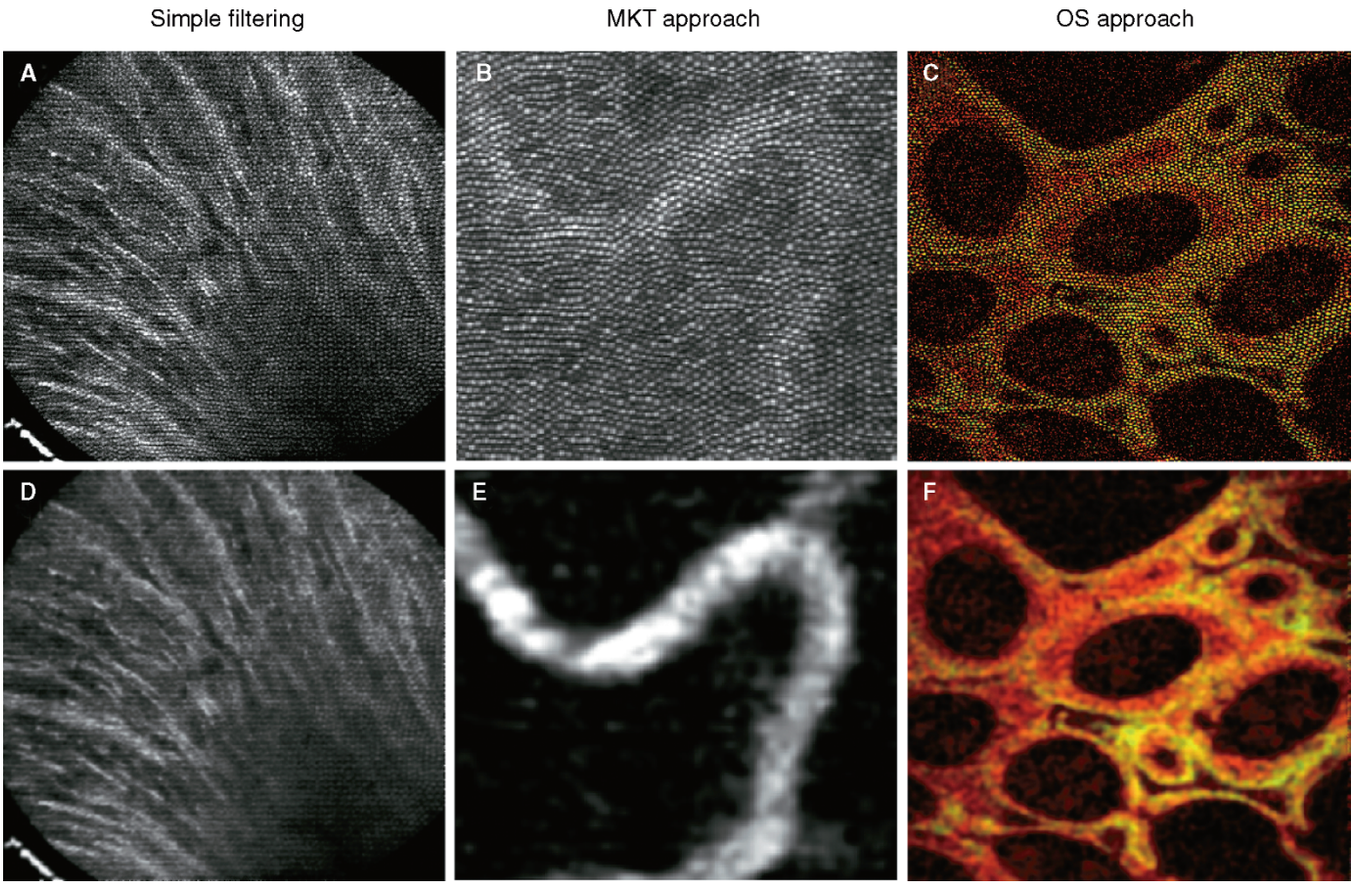

FIGURE 26.8. Software compensation of bundle artifacts. The pattern formed by the structure of the fiber bundle can be reduced using various software approaches. Simple spatial filtering can soften the bundle artifact, but significantly degrades resolution and contrast: (A) raw image, (D) image filtered with four passes of a 5×5 pixel Gaussian blur. A better approach involves collecting a reference image of the bundle pattern to subtract artifacts such as bundle autofluorescence (C) raw image, (E) processed image. A combination of background subtraction, pixel dilation, and filtering was used to process image (C) and to produce image (E). Potential artifacts of each of these approaches must be considered in the context of how the distal optical sampling is represented by the raw data obtained by scanning the proximal end of the fiber bundle (particularly when this is optimized for maximum laser launch efficiency, which results in clear resolution of the bundle elements). [Images (B) and (E) courtesy of Mauna Kea Technologies, Paris, France. Images (A), (C), (D), and (F) courtesy of Optiscan, Melbourne, Australia.]

Scan Heads Based on Single Fibers with Miniature Scanning Mechanisms

The use of a single fiber acting as both the source and detection aperture offers contiguous sampling of the imaging plane comparable to that offered by conventional scanning mirrors. However, the requirement to miniaturize a scanning mechanism for incorporation into the probe tip presents substantial technical challenges. Several approaches have been taken and practical devices have been realized, some of which are diagrammed in Figure 26.7. Scanning mechanisms include electromagnetic or piezoelectric scanning of the fiber itself, scanning of micro-mirrors, and scanning of a miniature lens.

Vibrating the Fiber Tip

In Figure 26.6(B) (Delaney *et al.*, 1993a), the output of a single-mode fiber is projected by a lens to form a collimated beam. This beam is focused by a second lens into an image plane in the specimen. These components form the confocal illumination path and the same fiber acts as the detection aperture for the return light. Scanning is implemented by moving the fiber tip, and being contiuous, this system suffers from none of the sampling problems that complicate the design of the fiber-bundle confocals.

All systems in which mechanical scanning is carried out at the tip require a counter-vibrating mass if small size and fast scan are desired. For example, the Optiscan system carries the fiber along one tine of a tuning fork to produce a resonant sinusoidal scan. The second tine moves in opposition balancing the reaction forces, which would otherwise move the case and result in visco-elastic damping by interaction with the tissue (Harris, patent). This approach has been used for a scanner that is 5 mm in diameter (see Fig. 26.10 inset) and forms the basis of a commercial clinical endomicroscope for human imaging (see Fig. 26.13).

Vibrating the Lens and Fiber

An alternative to scanning the fiber tip in front of static projection optics is from an endoscope image by mounting a very small lens on the tip of the fiber, so that the fiber output is focused to a point

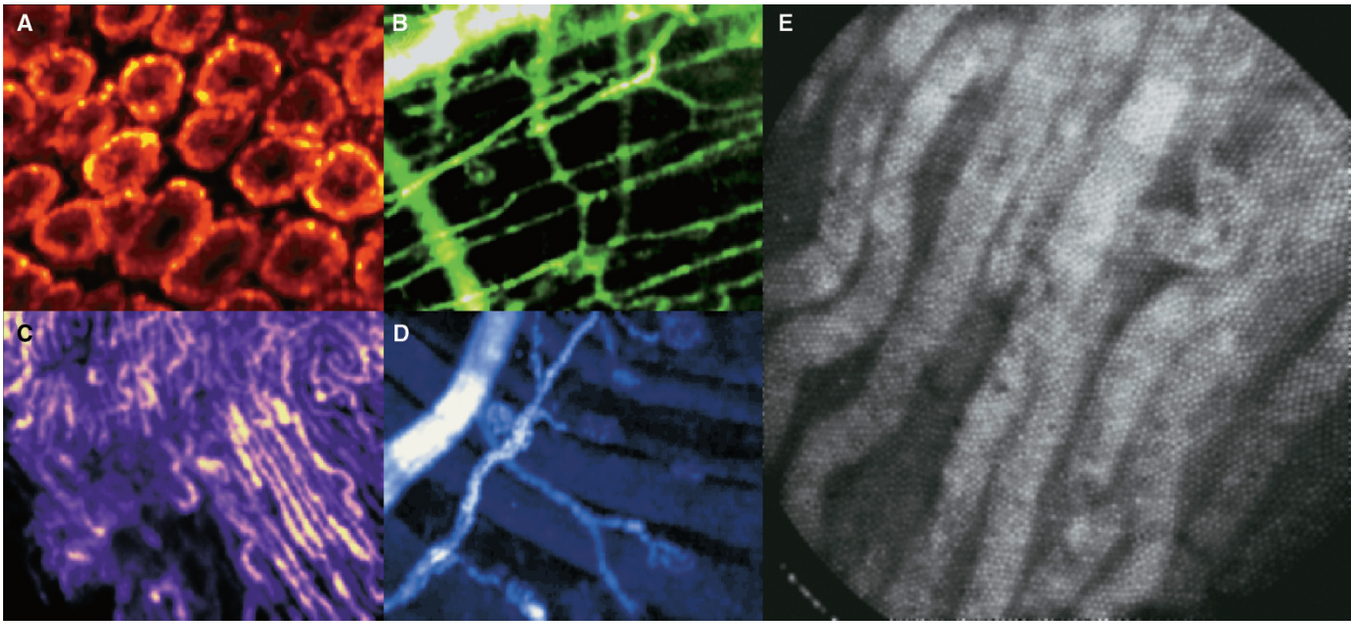

FIGURE 26.9. Imaging of animal tissue using miniature bundle systems. (A) Colonic crypts of a mouse mucosa after vital application of cresyl violet marking the cytoplasm and Syto13 marking the nuclei. Imaged endoscopically using the Cell~vizio, with a ProFlex S-1500, FOV: 400 × 280 µm. (B) Distal axon and motor endplates of a neuromuscular junction of a transgenically marked nervous system (Thy1-YFP mouse) with skeletal muscle fibers marked by topical application of Syto13. Imaged with the Cell~vizio and the direct contact of a ProFlex S-0650. (C) Proximal end of a cut sciatic nerve in a transgenic Thy1-YFP mouse, demonstrating the single-axon resolution. Imaged using a hand-held ProFlex S-0650. FOV: 400 × 280 µm. (D) Mouse cremaster microvasculature stained with FITC-albumin, injected intravenously. Imaged by the Cell~vizio and a hand-held ProFlex S-1500. FOV: 400 × 280 µm. (E) Rat kidney imaged with a prototype bundle contact tip, scanned using a desktop confocal microscope (Optiscan f900e). Field width, 400 µm. [Images (A), (B), and (C) courtesy of Igor Charvet and Paolo Meda CMU, Geneva, Switzerland, using equipment provided by Mauna Kea Technologies, Paris, France; (D) courtesy of Elisabeth Laemmel and Eric Vicaut, LEM, Paris, France; and (E) courtesy of Vladimir Dubaj and Andrew Wood, Swinburne University, Melbourne, Australia, utilizing equipment provided by Optiscan, Melbourne, Australia.]

near the fiber tip (Giniunas *et al*., 1991). Fused-fiber microlenses, gradient index lenses, and polymer lenses formed by the light leaving the fiber tip have all been tried. While offering appealing dimensions in both diameter and length, such systems are generally impractical due to their short working distance and/or narrow beam diameter.

Scanning with Micromirrors

Dickinsheets and Kino (1996) have demonstrated a system using two mirrors micro-machined from crystalline silicon. An optical design by Olympus using a single mirror held in a gimbal arrangement with torsion strips to provide resonance has also been demon-

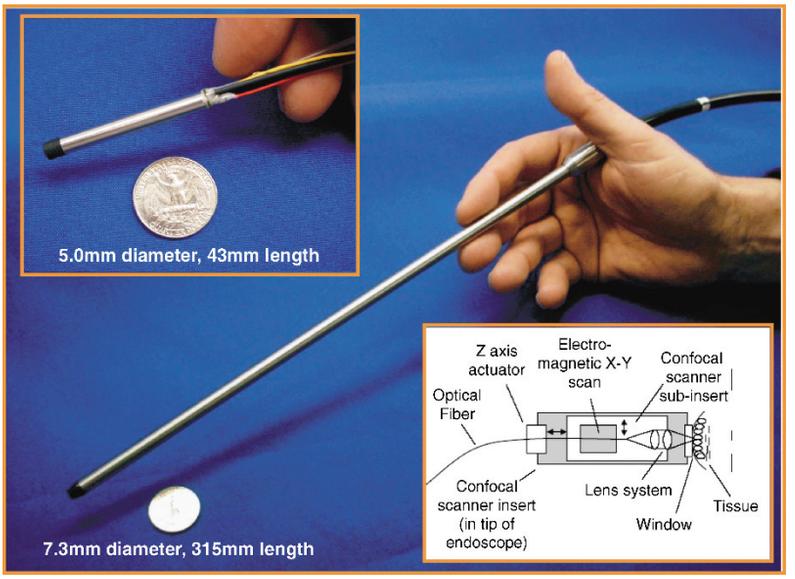

FIGURE 26.10. Miniature scanning-fiber confocal microscope scanner and rigid endoscope. The scanner (pictured inset top left) contains integrated raster scanning, a *z*-axis actuator, and projection objective optics encapsulated behind a fixed external window. The scanner produces 1024 × 1024 images at 1 frame per second. The objective NA is 0.55, providing lateral resolution of 0.7 µm and axial resolution of 7 µm. The external window is placed into contact with the sample and the *z*-axis actuator shifts the imaging depth from 0 to 250 µm relative to the contact surface. For *in vivo* microscopy, the scanner is packaged for the requirements of the application, in this case as a rigid arthroscope for minimally invasive surgical access to internal organs, or in the flexible endomicroscope shown in Figure 26.13. Images show a prototype made by Optiscan Pty Ltd, Melbourne, Australia. A schematic representation of the configuration of key components in the scanner is shown inset at lower right.

strated. The fiber emits light through a hole in the center of a primary catadioptic scanning mirror. The beam path is then folded by a secondary mirror on the surface of the first lens element (Murakami *et al.*, 2005).

Scanning Fiber Confocal Microscopes for *In Vivo* Imaging in Animals

The scanning fiber approach, described above and diagrammed in Figure 26.7, has been implemented in a 5 mm diameter scanner and packaged either as a hand-held probe or as a rigid endoscope, as shown in Figure 26.10. The devices also include an active *z*-axis actuator that moves the entire scanning mechanism and lens system relative to an imaging window incorporated into the end of the device. The window at the tip of the device is thus placed directly against the animal tissue of interest, rather than the tissue being placed onto a stage. Mechanical contact provides a high degree of stability, and the images are obtained interactively, with hand-held controls to adjust the imaging plane depth relative to the window surface. Sample images are presented in Figure 26.11, demonstrating practical imaging of microvascular, cellular, and subcellular structures *in vivo*.

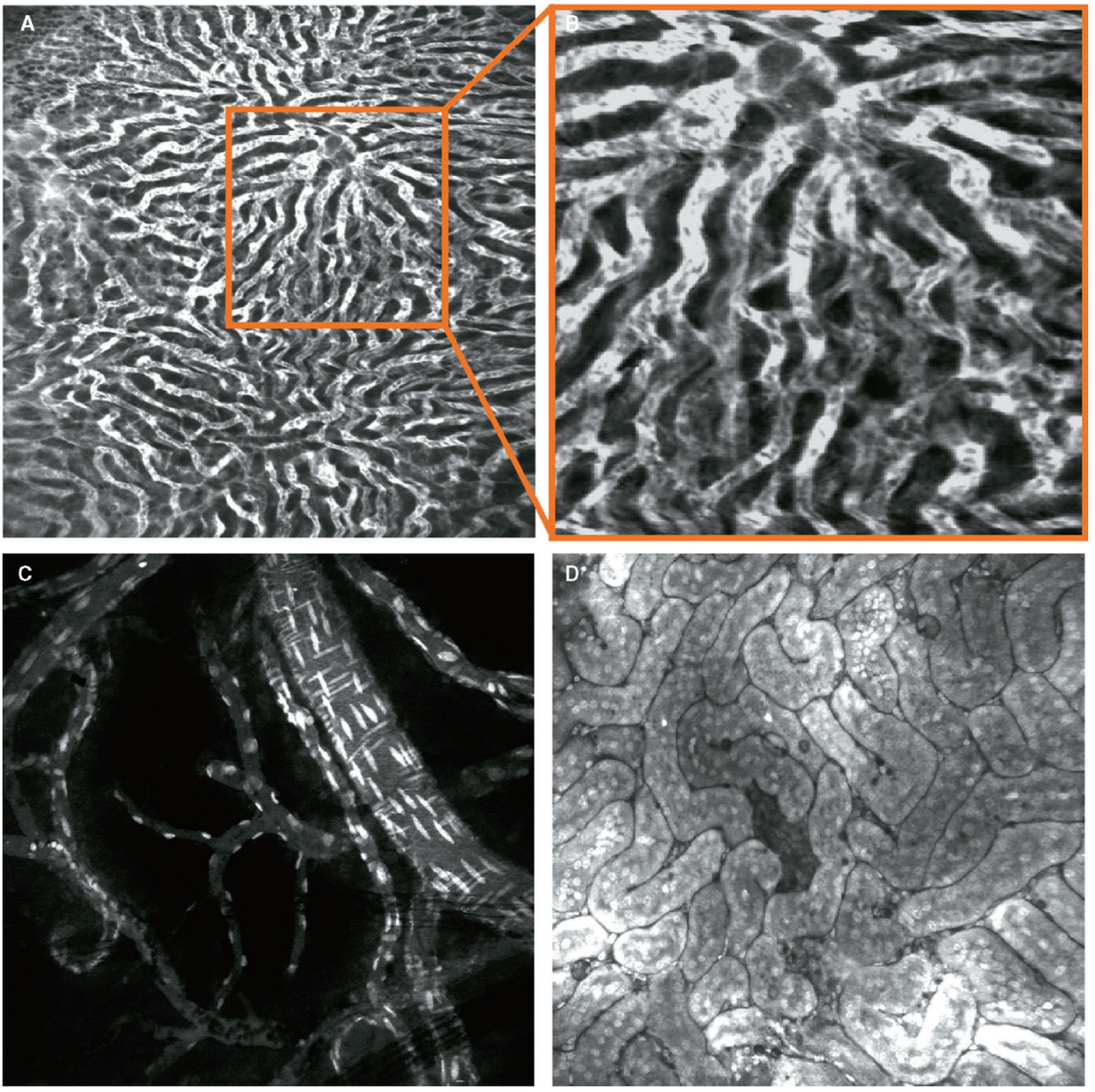

FIGURE 26.11. *In vivo* microscopy using the scanning fiber confocal microscope shown in Figure 26.10. (A) Mouse liver imaged following intravenous administration of FITC-dextran. (B) A region of this image zoomed in software to reveal the high information content and stability achievable *in vivo*. (C) Image of mouse brain following intravenous administration of Acriflavine, highlighting the longitudinal orientation of the nuclei of vascular epithelial cells versus the circumferential orientation of nuclei in vascular smooth muscle and muscle. All images are single 1 s scans at 1024 × 1024 pixel resolution, ex = 488 nm, det = 505–585 nm, and are courtesy of Dr. Ralf Kiesslich and Dr. Martin Goetz, Mainz University Hospital, Mainz, Germany.

IMPLEMENTATIONS FOR CLINICAL ENDOMICROSCOPY

Trends in medical diagnostics and therapeutics are towards point-of-care diagnostics and ever more rapid delivery of diagnostic information for guiding timely medical interventions. There has thus been growing interest in, and research into, various techniques for achieving non-invasive histologic imaging using miniaturized devices suitable for *in vivo* microscopy. In the past few years, numerous clinical applications have arisen, accelerated by the relatively recent development of prototypes and commercial systems certified for clinical investigation.

Three areas have involved substantial research and development effort and have been applied clinically:

Skin: Both non–fiber-optic and scanning fiber (Gonzalez and Tannous, 2002; Swindle *et al.*, 2003).

Cervix: Both fiber bundle and scanning fiber (Liang *et al.*, 2001; McLaren *et al.*, 2003; Fig. 26.12).

Gastrointestinal tract: The scanning fiber approach has resulted in a certified commercial gastrointestinal endomicroscope by Pentax, Japan (Delaney *et al.*, 1994b; Kiesslich *et al.*, 2004; see Fig. 26.14).

Clinical studies in all three areas have achieved diagnostic significance, suggesting a likely role for these technologies in clinical practice.

SUMMARY

Although to date relatively few developments have resulted in practical systems for clinical investigation, numerous ongoing efforts are aimed at achieving clinical confocal microscopy, and

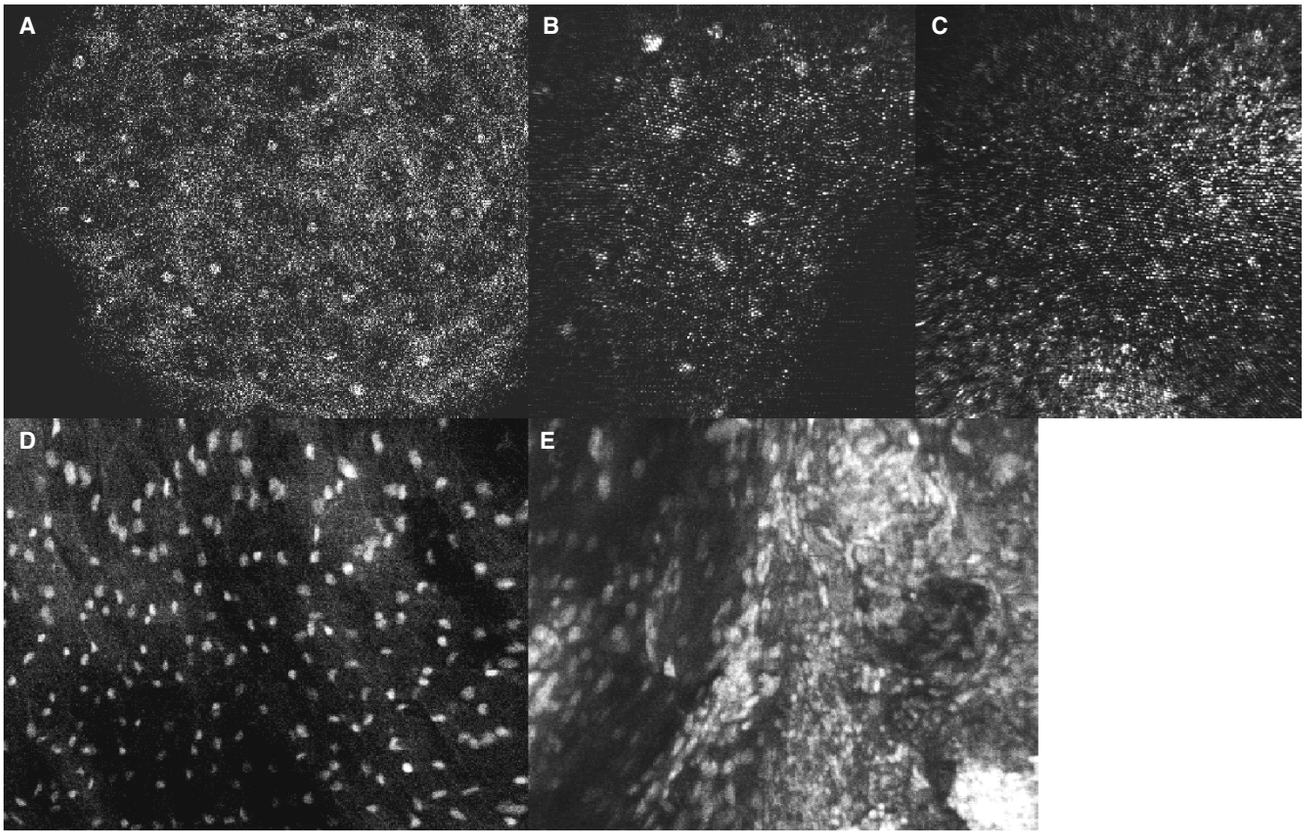

FIGURE 26.12. Imaging of the human cervix using miniature confocal microscope heads. (A) The *in vitro* images of cervical epithelium obtained with a reflectance confocal microscope demonstrates the ability to resolve cellular and nuclear structures in whole tissues. This epi-illumination confocal microscope consists of an 810 nm continuous-wave diode laser, a pair of galvanometer scanning mirrors, a scan lens, and a 25 × 0.8 NA water-immersion objective lens. The measured lateral and axial resolution of this system are 0.8 and 2 to 3 µm, respectively. The focus plane is 50 µm below the surface, the field width ~460. (B, C) *In vivo* fiber-optic confocal microscope backscattered light images of cervical epithelium classified as (A) normal and (B) abnormal, CIN II/III at histologic examination. FOV ~200 × 200 µm. The prototype constructed for this study scans 1064 nm continuous illumination from a Nd : YAG laser focused into a 30,000-fiber coherent imaging bundle (average core diameter 4 µm, average pitch 7 µm, fiber NA 0.3). A miniature objective lens at the distal tip has a back NA of 0.3 and an objective NA of 1.0. Specular reflection from the fiber surfaces is reduced by a polarizing beam-splitter, index-matching oil at both fiber bundle surfaces, and a 7° angle polish on the distal fiber bundle surface. The measured lateral and axial resolution for this fiber-optic confocal microscope are 2.1 and 3 to 6 µm, respectively. Images are obtained at 15 frames per second. Hydraulic suction is used to axially scan tissue through the fixed focal plane. The water is also used to reduce specular reflection from the surface of the tissue. (Images courtesy of Rebecca Richards-Kortum.) (D, E) Clinical *in vivo* imaging of human cervix using a fiber-scanning confocal microscope prototype similar to that pictured in Figure 26.10. Fluorescence images (excitation 488 nm, detection above 505 nm) following topical applications of 0.05% Acriflavine (FOV: 500 × 350 µm). Nuclei are well resolved, showing regular nuclear size, shape, and distribution in normal cervix (D) versus crowded distribution and irregular size and shape of nuclei (E) in squamous cell carcinoma (diagnoses provided by conventional histopathological assessment of biopsies). (Images courtesy of Dr. Jeffrey Tan, Royal Women's Hospital, Melbourne, Australia.)

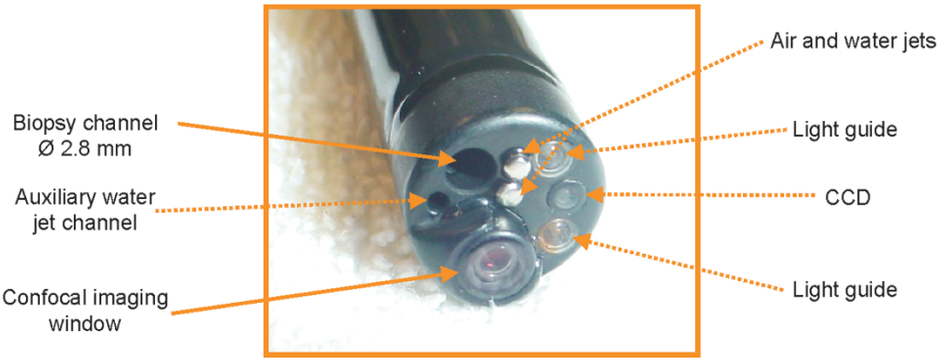

FIGURE 26.13. Clinical endomicroscope distal tip. The single-fiber scanner shown in Figure 26.10 has been incorporated into a clinical endomicroscopy system by Pentax Corporation, Medical Division (Tokyo, Japan). The distal tip is 12.8 mm in diameter, and accommodates the conventional endoscope components and functions (labeled) for macroscopic imaging, illumination, biopsy suction, spraying, and articulation. The confocal scanner protrudes by several millimeters, and appears within the corner of the conventional charge-coupled device (CCD) view, thus allowing the endoscopist to target it to specific locations on the tissue. (Image courtesy of Pentax Corporation.)

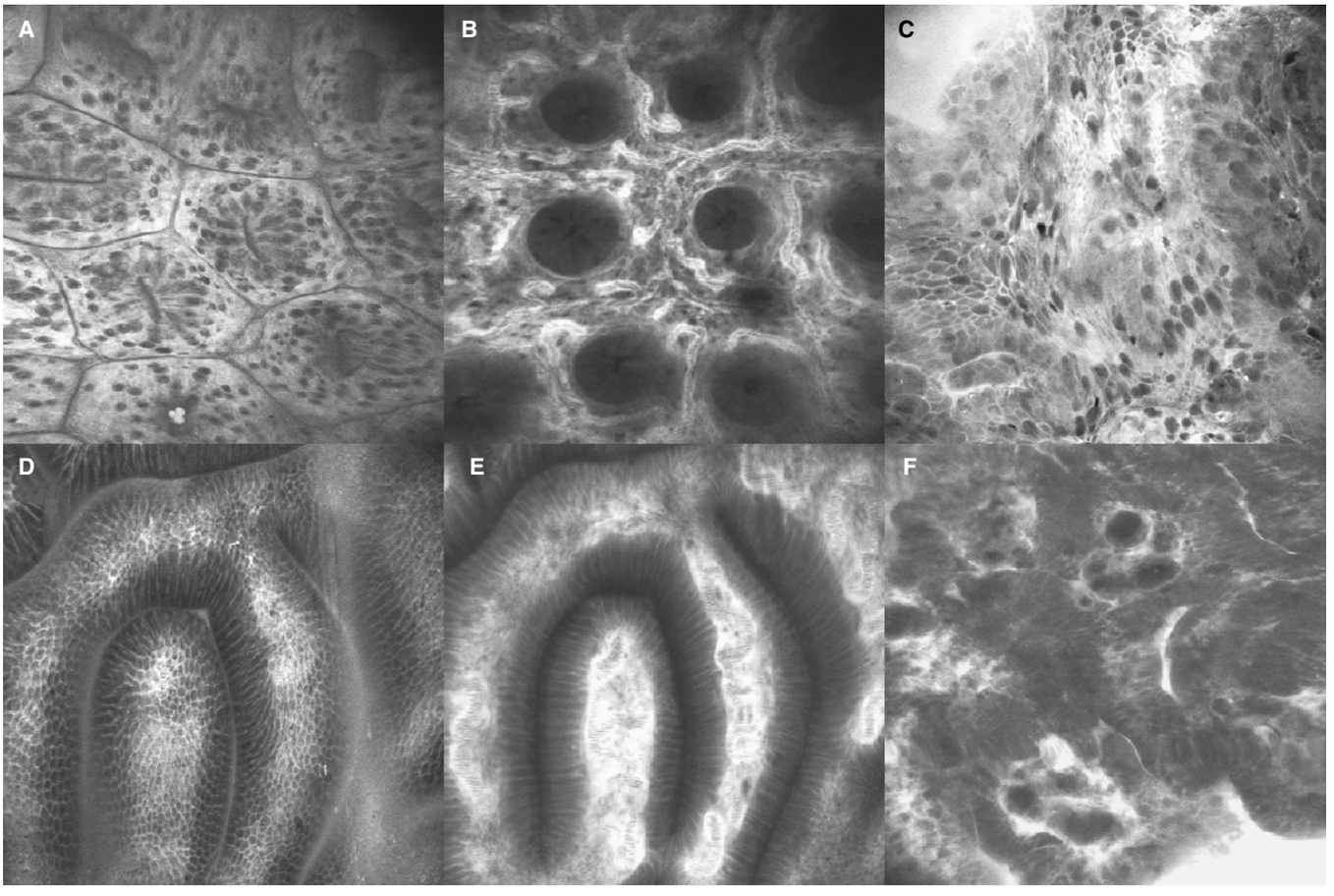

FIGURE 26.14. Confocal imaging of the human gastrointestinal tract in patients undergoing clinical endoscopy. (A–C) Colonic mucosa. (A) Crypt architecture, goblet cells, and epithelial cells in the plane of the superficial epithlelium. (B) Subsurface microvasculature surrounded by the collagen matrix of the *lamina propria*, 50 µm beneath the tissue surface, presenting the radial alignment of epithelial (including goblet) cells lining the crypt lumen. (C) Imaging of a rectal adenocarcinoma showing complete loss of crypt architecture, marked cellular pleomorphism, and patchy distribution of goblet cells throughout the image plane. (D–F) Human upper gastrointestinal images. (D) Surface epithelium and (E) hyper-vascularization of the *lamina propria* in a 66-year-old male with portal hypertension. (F) In a 62-year-old patient with Barrett's esophagus, a small region of neoplasia is imaged with the endomicroscope. [Images (A,B) courtesy of Prof. Adrian Polglase, Cabrini Monash University Department of Surgery, Melbourne, Australia. Images (C–F) courtesy of Dr. Ralf Kiesslich, Mainz University Hospital, Mainz, Germany.]

even the miniaturization of multi-photon microscopes suitable for *in vivo* microscopy. Thus, it is reasonable to expect that many other approaches will soon become practical tools for clinical and laboratory *in vivo* scanning optical microscopy.

ACKNOWLEDGMENTS

We are grateful to Mauna Kea Technologies (Paris, France) for Figure 26.8(A,B,D,E), to Igor Charvet and Paolo Meda (CMU, Geneva, Switzerland) for Figure 26.9(A,B,C), to Vladimir Dubaj and Andrew Wood (Swinburne University, Melbourne, Australia) for Figure 26.9(E), to Elisabeth Laemmel and Eric Vicaut (LEM, Paris, France) for Figure 26.9(D), to Dr. Ralf Kiesslich and Dr. Martin Goetz (Mainz University Hospital, Mainz, Germany) for Figure 26.11, to Rebecca Richards-Kortum (Rice University, Houston, TX) for Figure 26.12(A–C), to Dr. Jeffrey Tan (Royal Women's Hospital, Melbourne, Australia) for Figure 26.12(D,E), and to the Pentax Conporation (Tokyo, Japan) for Figures 26.13 and 26.14. Dr. Wendy McLaren provided invaluable assistance with the figures.

REFERENCES

Bjarklev, A., Broeng, J., and Bjarklev, A.S., 2003, *Photonic Crystal Fibers*, Kluwer Academic Publications, New York, pp. 1–298.

Cavé, C., Fourmeaux du Sartel, M., and Abrat, B., 2005, Fibered confocal fluorescence microscopy: A new tool to perform colonoscopy in mice, *Gastroenterology* 128(Suppl 2):A–249.

Delaney, P., Harris, M., and King, R., 1993a, Novel microscopy using fiber-optic confocal imaging and its suitability for subsurface blood vessel imaging *in vivo*, *Clin. Exp. Pharmacol. Physiol.* 20:197–198.

Delaney, P., Harris, M., and King, R., 1993b, Remote interrogation of objective lenses using a novel fiber-optic confocal microscope reduces movement artifacts, In: *The 1993 International Conference on Confocal Microscopy and 3D Image Processing Proceedings*, Sydney, Australia, p. 66.

Delaney, P., Harris, M., and King, R.G., 1994a, Fiber-optic laser scanning confocal microscope suitable for fluorescence imaging, *Appl. Opt.* 33:573–577.

Delaney, P., King, R., Lambert, J., and Harris, M., 1994b, Fiber-optic confocal imaging (FOCI) for subsurface imaging of the colon *in vivo*. *J. Anat.* 184:157–160.

Dickensheets, D.L., and Kino, 1996, A micromachine scanning confocal optical microscope, *Opt. Lett.* 21:764–766.

Ellis, G.W., 1985, Microscope illuminator with fiber-optic source integrator, *J. Cell. Biol.* 101:832a.

Fork, R., Martinez, O.E., and Gordon, J., 1984, Negative dispersion using pairs of prisms, *Opt. Lett*. 9:150.

Gmitro, A., and Aziz, D., 1993, Confocal microscopy through a fiber-optic imaging bundle, *Opt. Lett.* 18:565–567.

Giniunas, L., Juskaitis, R., and Shatalin,V., 1991, Scanning fiber-optic microscope, *Electron Lett.* 27:724–726.

Gonzalez, S., and Tannous, Z., 2002, Real-time, in vivo confocal reflectance microscopy of basal cell carcinoma, *J. Am. Acad. Dermatol*. 47:869–874.

Harris, M.R., UK Patent, GB 2,340,332. Granted 16-02-2000.

Harris, M., and Delaney P.M., US Patent, 5,926,592. Granted 20-07-1999.

Harris, M., and Delaney, P., US Patent no. 5,926,592.

Katzir, A., 1993, Applications of lasers in therapy and diagnosis, In: *Lasers and Optical Fibers in Medicine*, Academic Press, San Diego, California.

Kiesslich, R., Burg, J., Veith, M., Burg, J.,Vieth, M., Gnaendiger, J., Enders, M., Delaney, P., Polglase, A., McLaren, W., Janell, D., Thomas, S., Nafe, B., Galle, P., and Neurath, M., 2004, Confocal laser endoscopy for diagnosing intraepithelial neoplasias and colorectal cancer *in vivo*, *Gastroenterology* 127:706–713.

Kiesslich, R., et al., 2005, Diagnosing *Helicobacter pylori in vivo* by confocal laser endoscopy, *Gastroenterology*. Forthcoming.

Kimura, S., and Wilson, T., 1991, Confocal scanning optical microscope using single mode fiber for signal detection, *Appl. Opt.* 30:2143–2150.

Kino and Dickinsheets, D.L., US Patent no. 6,172,789.

Knight, J., Broeng, J., Birks, T., and Russel, P., 1998, Photonic bandgap guidance in optic fibers, *Science* 282:1476

Liang, C., Sung, K., Richards-Kortum, R., and Descour, M., 2001, Fiber confocal reflectance microscope (FCRM) for in-vivo imaging, *Opt. Express* 9:821–830.

McLaren, W., Tan, J., and Quinn, M., 2003, Detection of cervical neoplasia using non-invasive fibreoptic confocal microscopy, In: *Eurogin 2003* (J. Monsonego, ed.), Monduzzi Editore, Bologna, Italy, pp. 213–217.

Murakami, M., 2005, A miniature confocal optical scanning microscope for endoscopy, in MOEMS display and imaging systems III, (H. Urey and D.L. Dickensheets, eds.), *Proc SPIE.* 5721:119–131.

Ouzounov, D., Moll, K., Forster, M., Zipfel, W., Webb, W., and Gaeta, A., 2002, Delivery of nanojoule femtosecond pulses through large-core microsure fibers, *Opt. Lett.* 27:1513–1515.

Sharonov, S., Morjani, H., and Manfait, M., Confocal spectral imaging analysis: A new concept to study the drug distribution in a single living cancer cell, *Anticancer Res.* 12:1804.

Snyder, A., and Love, J., *Optical Waveguide Theory*, Chapman and Hall, London 1983.

Sung, K., Liang, C., Descour, M., Collier, T., Follen, M., and Richards-Kortum, R., 2002, Fiber-optic confocal reflectance microscope with miniature objective for *in vivo* imaging of human tissues, *IEEE Trans. Biomed. Eng*. 49:1168–1172.

Swindle, L., Thomas, S., Freeman, M., and Delaney, P., 2003, View of normal human skin in vivo as observed using fluorescent fiber-optic confocal microscopic imaging, J. *Invest. Dermatol*. 121:706–712.

Wilson, J., and Hawkes, J., *Optoelectronics. An Introduction*, 2nd ed., Prentice-Hall, Hemel Hempstead, UK Sects. 8.3.3, 8.3.4, and 8.5.2.

Wilson, T., Juskaitis, R., and Rimvydas, 1992, Confocal and differential microscopy using optical fiber detection. In: *Proceedings of SPIE-International Society for Optical Engineering*. Vol. 1660 pt 2.